Ultrafast ring-opening fragmentation dynamics of $C_6H_6{}^{3+}$ induced by electron-impact ionization

Jiaqi Zhou[1,2] Yutian Li,[1] Yingying Wang,[1] Shaokui Jia,[1] Xiaorui Xue,[1] Tao Yang[1] Zhen Zhang[1]
Alexander Dorn,[2] and Xueguang Ren[1,2,*]

[1]*MOE Key Laboratory for Nonequilibrium Synthesis and Modulation of Condensed Matter, School of Physics,*
Xi'an Jiaotong University, Xi'an 710049, China
[2]*Max-Planck-Institut für Kernphysik, Saupfercheckweg 1, 69117 Heidelberg, Germany*

The fragmentation dynamics of triply charged benzene $[(C_6H_6)^{3+}]$ induced by 260 eV electron-impact ionization are investigated using a multiparticle coincidence momentum spectrometer. By measuring three fragment ions and one outgoing electron in quadruple coincidence, we identify the complete three-body dissociation channels of $CH_2{}^+ + C_2H_3{}^+ + C_3H^+$, $CH_3{}^+ + C_2H_2{}^+ + C_3H^+$, and $C_2H_2{}^+ + C_2H_2{}^+ + C_2H_2{}^+$. We determine the projectile-energy-loss spectra, Dalitz plots, Newton diagrams, momentum correlation maps, and kinetic-energy release for each fragmentation channel. The analysis of these spectra is supported by an *ab initio* molecular dynamics simulation, which provides a molecular movie of the dissociation process. Our study reveals sequential mechanisms for all three dissociation channels of $(C_6H_6)^{3+}$ trication, i.e., an ultrafast ring-opening reaction followed by two subsequent Coulomb-explosion processes.

I. INTRODUCTION

Six-membered aromatic rings are ubiquitous in chemistry. They play an important role as building blocks for the construction of a wide variety of compounds, such as polycyclic aromatic hydrocarbons and DNA nucleobases [1,2]. As a result, studying the molecular properties of aromatic molecules can lead to a better understanding of various phenomena in chemical and biological systems [3,4]. In recent years, there has been considerable research efforts focusing on the ring-opening dynamics of aromatic molecules induced by photoexcitation [5–11] as they are relevant to many key reactions in biochemistry, such as the photobiological synthesis of vitamin D_3 in human skin [12,13]. When these molecules are transferred to higher excited states or even ionized, more complex ring-opening reactions can be initiated, such as successive ring-breaking and dissociation processes.

Benzene (C_6H_6) is an archetypal aromatic molecule. The ionization and subsequent dissociation of benzene can produce various isomers, which have been discovered to exist in the interstellar medium, and such radical ions may be an important source for many smaller carbonaceous fragments in space [14,15]. Therefore, understanding the dissociation dynamics of C_6H_6 in the highly charged state is of significant interest for elucidating how these radical species

arise. Numerous efforts have been devoted to investigating the fragmentation dynamics of benzene dications in which various dissociation pathways, including hydrogen migration channels, have been identified [16–22]. Much less attention has been paid to the dissociation processes of triply-charged benzene, in particular to the three-body Coulomb-explosion dynamics, even though the possibility to detect all fragments could help us to get very detailed insight into the dissociation mechanisms, such as sequential and concerted pathways [23–27].

In the present work, we report a joint experimental and theoretical study of the three-body fragmentation dynamics of $C_6H_6{}^{3+}$. Different from the previous experiment conducted with few-cycle intense laser pulses [28], here, the tricationic $C_6H_6{}^{3+}$ is produced by electron impact. Therefore, while a strong laser field can modify the initial neutral molecule [29] as well as the evolution of the final ion, here, we have an unperturbed initial state, and the ion undergoes a field-free evolution after ionization. Furthermore, the understanding of electron-initiated processes is of great relevance to many research fields ranging from astrochemistry and plasma physics to radiation biology [30–33]. The complete three-body Coulomb-explosion processes of $C_6H_6{}^{3+}$ were measured using a multiparticle coincidence momentum spectrometer (reaction microscope) in which the momentum vectors and, consequently, kinetic energies of all three fragment ions and one outgoing electron are determined. The measurements of energy-loss spectra, momentum correlation maps between two fragment ions, and kinetic-energy-release (KER) spectra, Dalitz plots [34], and Newton diagrams [35] for three-body dissociation, accompanied by *ab initio* molecular dynamics simulations, allow us to examine comprehensively the fragmentation dynamics and thus provide a detailed picture of the dissociation mechanisms of $C_6H_6{}^{3+}$.

*renxueguang@xjtu.edu.cn

II. EXPERIMENTAL METHODS

The experiments were performed using a reaction microscope which was particularly designed for electron-collision experiments. Details about the experimental setup have been given elsewhere [36,37]. Here, a brief description is introduced. A pulsed electron beam with an energy of 260 eV is crossed with a supersonic gas jet, which can cause the ionization of the target with a small fraction of multiple ionization. Here, the projectile energy of 260 eV is chosen due to the relatively high triple-ionization cross section, and also we want to exclude the possible contribution from carbon *K*-shell ionization and subsequent autoionization processes which can be initiated at projectile energy above 285 eV. The pulsed projectile beam is emitted from an electron gun in which a tantalum photocathode is irradiated by a pulsed ultraviolet laser beam. The wavelength, repetition rate, and pulse width of the laser beam are 266 nm, 40 kHz, and 0.5 ns, respectively. The benzene gas jet was generated by the supersonic gas expansion of helium gas (stagnation pressure of 1 bar) seeded with benzene vapor through a nozzle with a diameter of 30 μm and the two-stage differential pumping system. The three cations originating from the Coulomb explosion of $C_6H_6^{3+}$ and one outgoing electron are detected in quadruple coincidence. They are extracted from the target region by means of uniform electric and magnetic fields in opposite directions and projected onto two position- and time-sensitive microchannel plate detectors with hexagonal delay-line position readout. For each detected particle the three-dimensional momentum vector is reconstructed from the time of flight and the position of impact on the detector. To maximize the acceptance for molecular ion fragments with comparably high momentum, the initial electric extraction field of 1.0 V cm^{-1} is ramped up to 26 V cm^{-1} after 400 ns when the electrons have reached the detector.

III. THEORETICAL METHODS

Our *ab initio* molecular dynamics (AIMD) simulations were performed under the extended Lagrangian molecular dynamics scheme adopting the so-called atom-centered density-matrix-propagation method [38–40] using the density-functional-theory method at the Becke three-parameters Lee-Yang-Parr (B3LYP) functional and correlation-consistent polarized valence double zeta (cc-pVDZ) basis set level. We first sampled the molecular geometries and the velocities of every atom in the neutral C_6H_6 by the quasiclassical fixed normal-mode sampling method [38] for a temperature of about 30 K at which the populations of the initial rovibrational states were determined by Boltzmann distributions. Here, the fragmentation pathways were simulated starting from the vertical transition to the triply charged benzene ions and up to 2500-fs propagation time with a step size of 0.5 fs.

The triple-ionization threshold of benzene was calculated using the coupled cluster theory with single, double, and perturbative triples [CCSD(T)] method and augmented correlation-consistent polarized valence triple zeta (aug-cc-pVTZ) basis set [41], which amounts to about 47.5 eV, as shown by the vertical arrow in Fig. 1. The present Coulomb-explosion channels are induced upon the population of electronic excited states of benzene trication [42]. In the
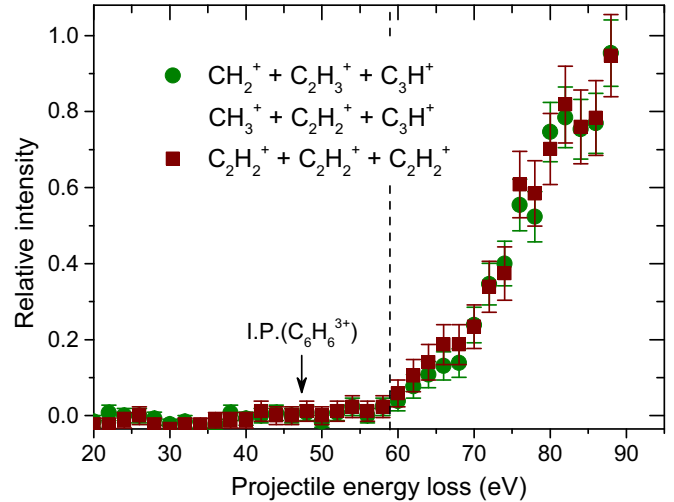

FIG. 1. The projectile-energy-loss spectra for the three considered fragmentation channels. The spectra are normalized to unity at the maximum.

simulations, the Coulomb explosion of the electronic excited state of $C_6H_6^{3+}$ is initiated by imparting an amount of internal energy (0.4 hartree) into the electronic ground state of the system. This is an approximate way to consider the electronic excited state in the calculations. The amount of internal energy is adapted to the measured projectile-energy-loss spectra, defined as the incident projectile energy E_0 minus the scattered electron energy E_1 ($E_{loss} = E_0 - E_1$). The spectra show onsets at $E_{loss} \sim 59$ eV (see the dashed line in Fig. 1). This supports the idea that the fragmentation processes originate from the electronic excited state of tricationic benzene. This excess energy can be converted into the vibrational energy of the molecule through the fast internal conversion leading to dissociation. The simulations at each step were performed with the converged self-consistent-field results. This is an effective way to maintain the dynamics on a given electronic state, i.e., equivalent to the Born-Oppenheimer surface [38–40]. We calculated 300 trajectories for the molecular dynamics simulations in which only one trajectory is obtained for the complete three-body dissociation channels, probably due to the high-energy barriers. We calculated the sum of the center-of-mass energies of three fragment ions at $t = 2500$ fs, which amount to 11.4 and 9.9 eV for the $CH_2^+ + C_2H_3^+ + C_3H^+$ and $CH_3^+ + C_2H_2^+ + C_3H^+$ channels, respectively. The total KER can be obtained by adding the remaining Coulomb potential energy, which is about 0.3 eV for both channels [43]. All calculations were carried out with the GAUSSIAN 16 suite of programs [44].

IV. RESULTS AND DISCUSSION

In this work, we focus on three complete three-body Coulomb-explosion channels, which are described as

$$(i): \quad C_6H_6^{3+} \rightarrow CH_2^+ + C_2H_3^+ + C_3H^+,$$

$$(ii): \quad C_6H_6^{3+} \rightarrow CH_3^+ + C_2H_2^+ + C_3H^+,$$

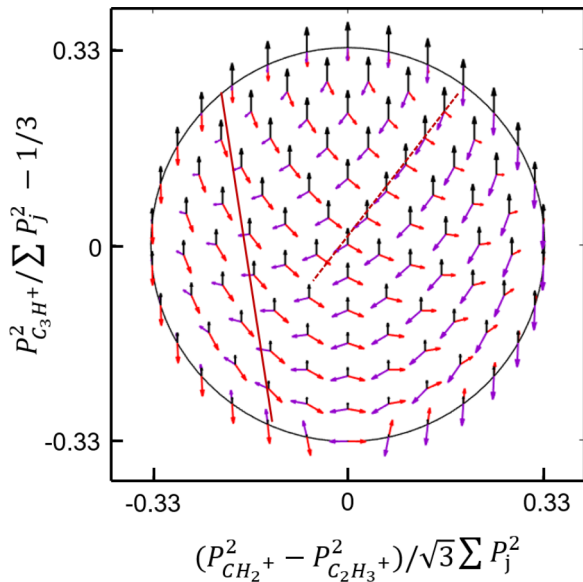$$(iii): \quad C_6H_6^{3+} \rightarrow C_2H_2^+ + C_2H_2^+ + C_2H_2^+.$$

FIG. 2. The calculated Dalitz plot considered for channel (i). The purple, red, and black arrows represent the momentum vectors of CH_2^+, $C_2H_3^+$, and C_3H^+, respectively. The dissociation characteristics of the events labeled by solid and dashed lines correspond to the features in Fig. 3(a) marked by the same lines.

The ion yield ratios are determined to be 1 : 1.17 : 1.20 for channels (i)–(iii), respectively. The measured projectile-energy-loss spectra indicate that the triply charged $C_6H_6^{3+}$ cations are created most likely through a direct inner-shell ionization [45] upon electron impact and subsequent Auger processes [27,46,47].

In the following, we use the Dalitz plot, Newton diagram, and momentum correlation map to study the mechanistic details of the three-body fragmentation dynamics. The Dalitz plot shows a probability density in terms of the vector correlation of the three fragment ions, i.e.,

$$\frac{P_a^2}{\sum P_j^2} - \frac{1}{3}$$

vs

$$\frac{P_b^2 - P_c^2}{\sqrt{3} \sum P_j^2},$$

where P_j, with $j = a, b, c$, is the momentum of each fragment.

The experimental Dalitz plot of channel (i) is presented in Fig. 3(a), which shows one intense stripe and one weak stripe, marked by the solid and dashed lines, respectively. As shown in Fig. 2, each point in the calculated Dalitz plot corresponds to a specific momentum correlation pattern among the three fragments for channel (i). The calculated pattern for channel (ii) is similar to that of channel (i), with a slight difference in the mass of the fragments. The momentum value of $C_2H_3^+$, i.e., the length of the red arrows, is constant along the solid line, which corresponds to the intense stripe shown in Fig. 3(a). However, the momentum value of CH_2^+ shows inverse dependence on the value of C_3H^+; that is, when one momentum increases, the other one decreases. These features indicate a sequential breakup channel for the strip structures in
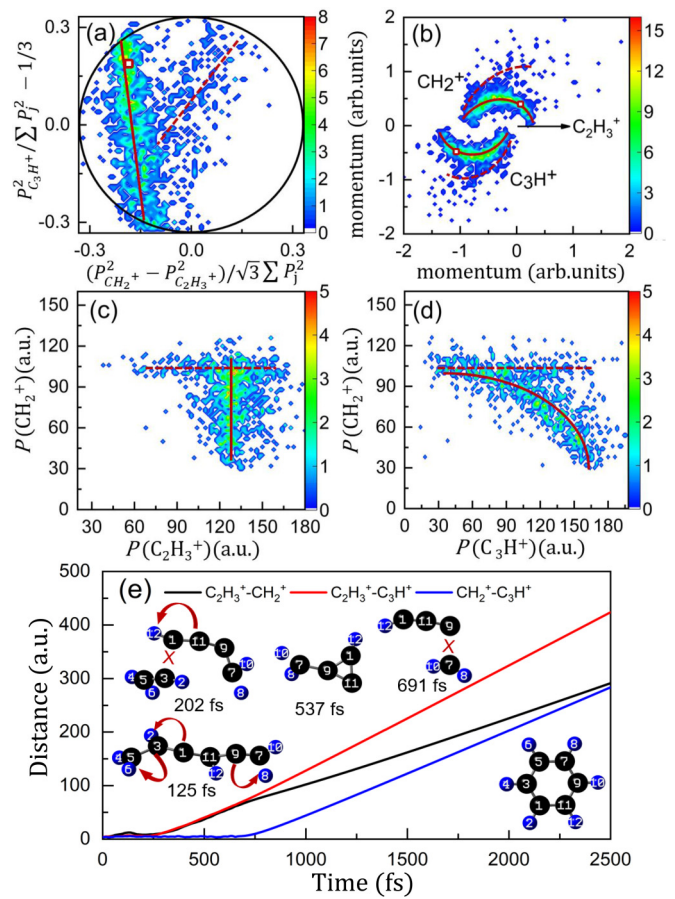

FIG. 3. (a) Experimental Dalitz plot and (b) Newton diagram of channel (i) in which the AIMD simulation is shown by the open squares. Momentum correlation spectra (c) between $C_2H_3^+$ and CH_2^+ and (d) between C_3H^+ and CH_2^+. The solid and dashed lines correspond to either $C_2H_3^+$ and CH_2^+ being emitted in the first Coulomb explosion, respectively. (e) Center-of-mass distances between different moieties within the $C_6H_6^{3+}$ ion as a function of evolution time after ionization. The molecular structures at specific evolution times are presented in the insets, which include ring opening and Coulomb explosion, with possible hydrogen migration marked by the curved arrows.

Fig. 3(a). To get more insight into the fragmentation dynamics, the data are displayed as a Newton diagram in Fig. 3(b). Here, the momentum vector of the $C_2H_3^+$ ion is represented by an arrow along the horizontal axis fixed to 1.0 arbitrary unit. The momentum vectors of the CH_2^+ and C_3H^+ cations are normalized to the momentum vector of the $C_2H_3^+$ ion and mapped in the upper and lower halves of the diagram, respectively. It can be seen that the momenta of CH_2^+ and C_3H^+ fragments are located on two semicircle patterns marked by solid and dashed lines, which are clear signatures of sequential dissociation [48].

Additionally, the two-dimensional momentum correlation maps between fragment ions are presented in Figs. 3(c) and 3(d) to distinguish the fragmentation sequences. Both spectra show straight-line distributions along the x axis or y axis that are a characteristic feature of the sequential process [49]. As an example, the distribution along the y axis in Fig. 3(c)

indicates that the momentum of the $C_2H_3^+$ ion is constant, while the momentum of the CH_2^+ ion shows a wide distribution. This means that the emission of $C_2H_3^+$ is independent of the formation of C_3H^+ and CH_2^+, suggesting that the sequential breakup proceeds as

$$C_6H_6^{3+} \rightarrow C_2H_3^+ + C_4H_3^{2+}, \tag{1}$$

$$C_4H_3^{2+} \rightarrow CH_2^+ + C_3H^+. \tag{2}$$
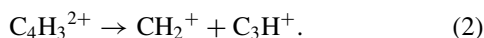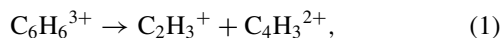
It is worth noting that CH_2^+ can also be emitted first, and the dissociative pathway can be described as

$$C_6H_6^{3+} \rightarrow CH_2^+ + C_5H_4^{2+}, \tag{3}$$

$$C_5H_4^{2+} \rightarrow C_2H_3^+ + C_3H^+. \tag{4}$$
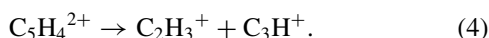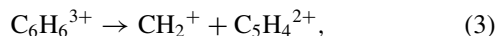
In this channel, either $C_2H_3^+$ (solid line) or CH_2^+ (dashed line) may depart from the parent ion in the first step of dissociation. After a time delay, the second Coulomb explosion occurs; that is, the intermediate $C_4H_3^{2+}$ ($C_5H_4^{2+}$) further dissociates into CH_2^+ ($C_2H_3^+$) and C_3H^+ cations. The rotation of the intermediate group relative to the first emitted cation causes the circular structures in the Newton diagram in Fig. 3(b).

Moreover, the C_3H^+ cation is not observed in the first dissociation process. The ring-opening reaction occurs in the first step, forming a chain precursor ion, e.g., $(C_2H_3\text{-}C_3H\text{-}CH_2)^{3+}$. In the next step, one of the moieties located at both ends of the carbon chain, i.e., $C_2H_3^+$ or CH_2^+, is emitted, leading to the first Coulomb explosion, as described in Eqs. (1) and (3). However, the departure of the middle C_3H^+ would cause simultaneous dissociation. This concerted fragmentation process is not observed in the experiment.

A possible reaction path for channel (i) has been restored with the help of our AIMD simulations. As shown in Fig. 3(e), the molecular dissociation is visualized by plotting the center-of-mass distances of the groups within the $C_6H_6^{3+}$ ion as a function of time. To facilitate the discussion, all atoms in the benzene molecule are labeled with different numbers, as shown in the molecular structure in the lower right corner of Fig. 3(e). The ultrafast ring-opening and hydrogen-migration reactions lead to the formation of a chained $C_6H_6^{3+}$ trication with the C_2H_3 and CH_2 groups located at the two ends of the molecular chain; see the molecular structure at $t \sim 125$ fs. The first emission of either $C_2H_3^+$ or CH_2^+ can lead to the two dissociation pathways of channel (i) as described in Eqs. (1) and (3), respectively. In the present simulation, we observe the first explosion into the $C_2H_3^+ + C_4H_3^{2+}$ ion pair, occurring at $t \sim 200$ fs. The remaining $C_4H_3^{2+}$ dication can dissociate into $CH_2^+ + C_3H^+$ at about 700 fs. This pathway corresponds to the intense patterns (solid lines) in Figs. 3(a) and 3(b). The fragment momenta for the trajectory obtained by the AIMD simulation are presented by open squares in the Dalitz plot and Newton diagram, which agree well with the experimental results.

In addition to channel (i), another channel [channel (ii)] with a C_3H^+ fragment and therefore clear evidence of dihydrogen migration is also observed. Its Dalitz plot and Newton diagram are shown in Figs. 4(a) and 4(b), respectively. The Dalitz plot shows an oblique stripe, which is a signature of the
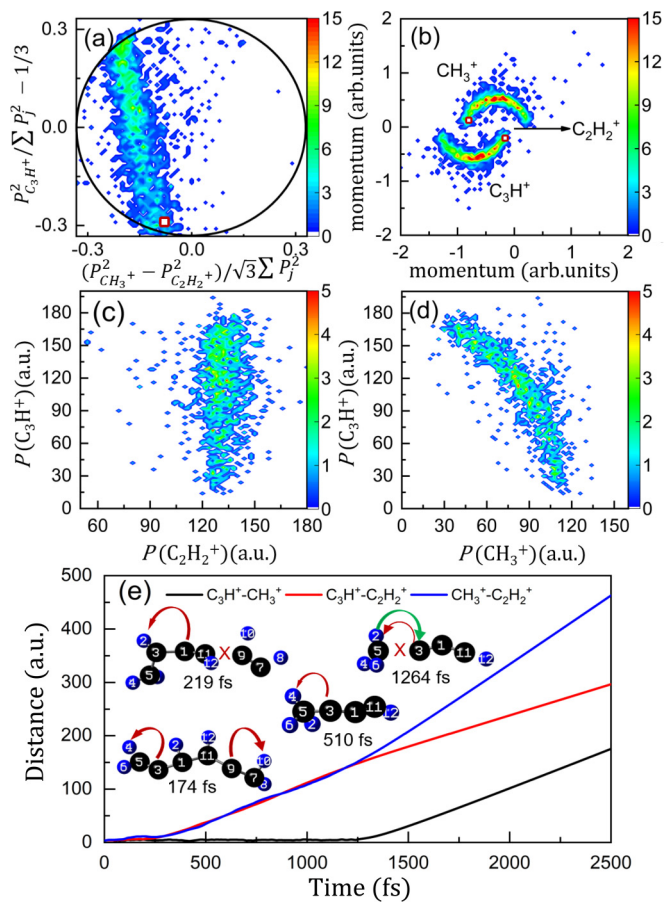

FIG. 4. (a) Experimental Dalitz plot and (b) Newton diagram of channel (ii) in which the AIMD simulation is shown by the open squares. Momentum correlation spectra (c) between $C_2H_2^+$ and C_3H^+ and (d) between CH_3^+ and C_3H^+. (e) Center-of-mass distances between different moieties within the $C_6H_6^{3+}$ ion as a function of evolution time after ionization.

sequential dissociation process. The two complete semicircle distributions in the Newton diagram also confirm this mechanism. The two-dimensional momentum correlation spectra, shown in Figs. 4(c) and 4(d), indicate that the $C_2H_2^+$ ion is emitted in the first dissociation process, and then the exploding $CH_3^+ + C_3H^+$ ion pair is formed in the second step. This sequential process can be described as

$$C_6H_6^{3+} \rightarrow C_2H_2^+ + C_4H_4^{2+}, \tag{5}$$

$$C_4H_4^{2+} \rightarrow CH_3^+ + C_3H^+. \tag{6}$$
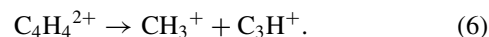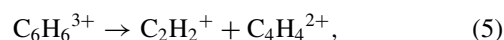
The AIMD calculated data for channel (ii) are also presented by open squares in Figs. 4(a) and 4(b), which are well within the experimental results for both Dalitz and Newton distributions, respectively. The dynamical evolution of $C_6H_6^{3+}$ is shown in Fig. 4(e), where the benzene trication experiences an ultrafast ring-opening reaction, i.e., a rapid rupture of one C-C bond, forming a chain structure followed by hydrogen migrations. Another C-C bond is broken at $t \sim 200$ fs, leading to the formation of $C_2H_2^+$ and $C_4H_4^{2+}$ fragments under the action of the Coulomb repulsive force.
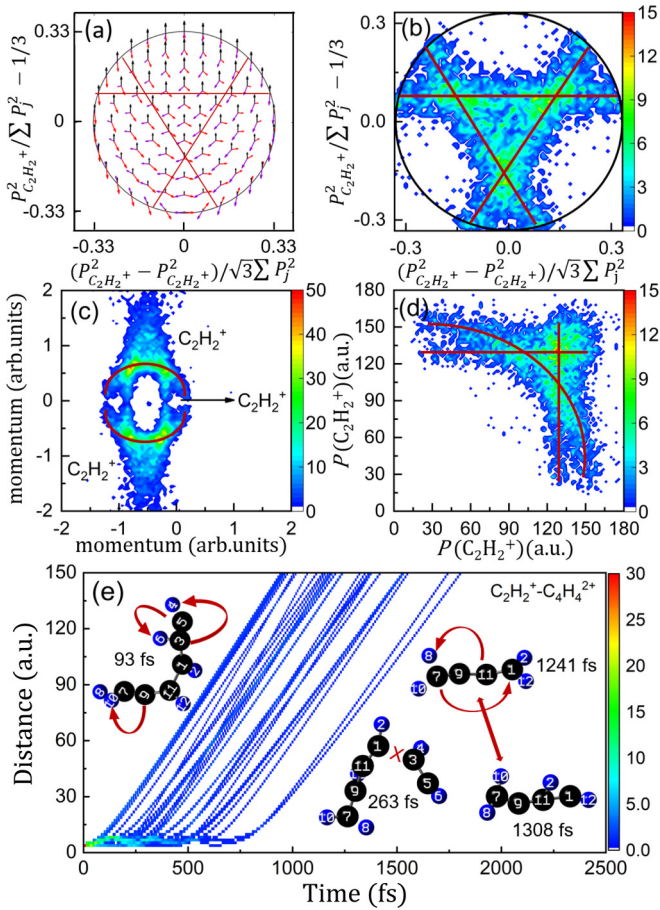
FIG. 5. (a) Calculated and (b) experimental Dalitz plots as well as (c) the Newton diagram of channel (iii). (d) Two-dimensional momentum correlation spectra between three $C_2H_2^+$ ions. (e) Center-of-mass distances between $C_2H_2^+$ and $C_4H_4^{2+}$ ions as a function of evolution time after ionization. Note that since the fragments are indistinguishable, p and p^2 randomly denote the momenta and the energies of the three $C_2H_2^+$ ions.

The second explosion occurs at $t \sim 1200$ fs, leading to the $CH_3^+ + C_3H^+$ ion pair.

The fragmentation dynamics for dissociation channel (iii), i.e., $C_6H_6^{3+} \rightarrow C_2H_2^+ + C_2H_2^+ + C_2H_2^+$, are shown in Fig. 5. Since the fragments are indistinguishable, P and P^2 randomly denote the momenta and energies of the three detected $C_2H_2^+$ ions. Figures 5(a) and 5(b) present the calculated and experimental Dalitz plots for this symmetric breakup channel, respectively. This channel exhibits three straight stripes marked by the solid lines forming a triangular pattern in the experimental Dalitz plot. The straight stripe distribution parallel to the x axis means that the kinetic energy of one $C_2H_2^+$ ion is independent of the others, which is a signature of a stepwise dissociation process. As shown in Fig. 5(c), the Newton diagram shows two semicircle distributions, which support the sequential dissociation mechanisms. The momentum correlation map, shown in Fig. 5(d), indicates that one $C_2H_2^+$ cation is emitted in the first dissociation process, i.e., the $C_2H_2^+ + C_4H_4^{2+}$ explosion described in Eq. (5). The $C_4H_4^{2+}$ dication fragments into two $C_2H_2^+$ cations in the

second dissociation step:

$$C_4H_4^{2+} \rightarrow C_2H_2^+ + C_2H_2^+. \tag{7}$$
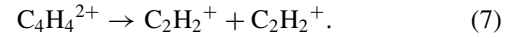
Our AIMD simulation reveals the possible pathways for the first Coulomb-explosion process of channel (iii), which are shown in Fig. 5(e). After the formation of the $C_6H_6^{3+}$ trication, ultrafast C-C bond breaking can take place, leading to the ring-opening reaction. The cyclic carbon ring expands into a chain structure, accompanied by hydrogen migrations, and forms two $C_2H_2^+$ branches connected at the two terminals of the carbon chain; see the molecular structure at $t \sim 93$ fs in Fig. 5(e). One of the two $C_2H_2^+$ branches is emitted in the first dissociation process that occurs at 100–800 fs; see the trajectories in Fig. 5(e). In the subsequent evolution there are still hydrogen migrations; see the molecular structures at later times. The intermediate $C_4H_4^{2+}$ may further dissociate into a $C_2H_2^+ + C_2H_2^+$ ion pair. However, the second dissociation step is not obtained within the simulated 2500-fs time range, probably due to the high potential barrier of this reaction [42].

Our simulations show that one C-C bond in the $C_6H_6^{3+}$ benzene ring undergoes a rapid rupture (50–100 fs), and the ring-opening reaction is considered to be complete at about 100–150 fs, which forms a molecular chain structure involving various hydrogen migrations. As the sequential mechanisms are determined for all three fragmentation channels, the KER for the first two-body dissociation process E_a can be calculated using the momentum of the first emitted cation together with the momentum-conservation law. The energies of E_a for the three different two-body fragmentation processes, $C_2H_3^+ + C_4H_3^{2+}$, $CH_2^+ + C_5H_4^{2+}$, and $C_2H_2^+ + C_4H_4^{2+}$, are determined to be 7.1, 6.5, and 7.3 eV, respectively, which are in rather good agreement with the potential-energy calculations for $C_6H_6^{3+}$ [28,42]. The measured total KERs (see Fig. 6) for channels (ii) and (iii) show peak values of about 11.0 and 12.1 eV, respectively, which are in good agreement with the peak values of about 11.4 and 12.5 eV obtained by intense laser-induced ionization [28]. For channel (i), the total KER distribution shows a peak value of about 10.5 eV, which is also in good agreement with the laser experiment [28]. The simulated KERs for channels (i) and (ii), shown by the vertical arrows in Fig. 6, lie well within the range of experimental KER distributions. Hence, our AIMD simulations are justified together with the good agreement between experiment and AIMD simulations for the Dalitz and Newton spectra shown in Figs. 3 and 4.

V. CONCLUSIONS

In summary, we have studied the ring-opening fragmentation dynamics of $C_6H_6^{3+}$ induced by electron-impact ionization ($E_0 = 260$ eV) using a multiparticle momentum spectrometer. The complete three-body dissociation channels, i.e., (i) $CH_2^+ + C_2H_3^+ + C_3H^+$, (ii) $CH_3^+ + C_2H_2^+ + C_3H^+$, and (iii) $C_2H_2^+ + C_2H_2^+ + C_2H_2^+$, and their energy-loss spectra are identified by coincident measurements of three fragment ions and one outgoing electron. The fragmentation dynamics of these three channels are analyzed using Dalitz plots, Newton diagrams, and momentum correlation spectra. These results, supported by our AIMD simulations,
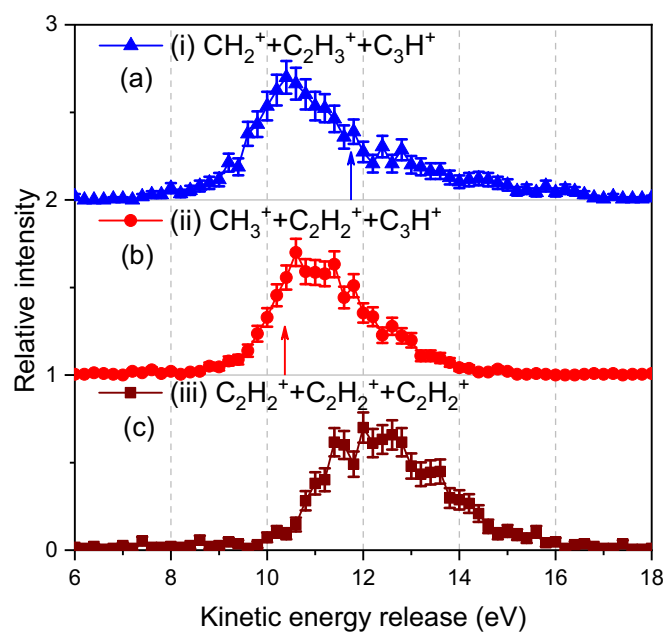
FIG. 6. Measured kinetic-energy-release (KER) spectra for all three dissociation channels. The red and blue vertical arrows represent the simulated KER values.

might be a lack of suitable transition states, which can lead to a direct pathway for symmetric dissociation of $C_6H_6^{3+}$ into three $C_2H_2^+$ cations.

The present study shows that the tricationic $C_6H_6^{3+}$ undergoes an ultrafast ring-opening reaction in the first step. This forms a chain structure of $C_6H_6^{3+}$ with various hydrogen migrations. Then the trication undergoes the first Coulomb-explosion process, leading to the cation and dication species. Finally, the second Coulomb explosion can occur in the dicationic species, which then forms a pair of cations. The measured total KERs of all three channels are in good agreement with the previous laser experiment. The present AIMD simulation provides a real-time dynamical picture of the fragmentation channels, which agree well with the experimental Dalitz plot, Newton diagram, and KER distribution. Our study provides detailed information on the ring-opening fragmentation dynamics of the triply ionized benzene molecule initiated by electrons and thus expands our understanding of radiation chemistry and biology.

ACKNOWLEDGMENTS

reveal the sequential mechanisms for all dissociation channels. The present results are in contrast to studies of small molecules where the concerted dissociation mechanisms were found to be dominant [23–26]. According to theory [42], there

[1] L. Zhao, R. I. Kaiser, B. Xu, U. Ablikim, M. Ahmed, M. V. Zagidullin, V. N. Azyazov, A. H. Howlader, S. F. Wnuk, and A. M. Mebel, VUV photoionization study of the formation of the simplest polycyclic aromatic hydrocarbon: Naphthalene ($C_{10}H_8$), J. Phys. Chem. Lett. **9**, 2620 (2018).

[2] M. Barbatti, A. J. A. Aquino, J. J. Szymczak, D. Nachtigallová, P. Hobza, and H. Lischka, Relaxation mechanisms of UV-photoexcited DNA and RNA nucleobases, Proc. Natl. Acad. Sci. USA **107**, 21453 (2010).

[3] L. M. Salonen, M. Ellermann, and F. Diederich, Aromatic rings in chemical and biological recognition: Energetics and structures, Angew. Chem., Int. Ed. **50**, 4808 (2011).

[4] R. I. Kaiser, D. S. Parker, and A. M. Mebel, Reaction dynamics in astrochemistry: Low-temperature pathways to polycyclic aromatic hydrocarbons in the interstellar medium, Annu. Rev. Phys. Chem. **66**, 43 (2015).

[5] J. M. Ruddock, H. Yong, B. Stankus, W. Du, N. Goff, Y. Chang, A. Odate, A. M. Carrascosa, D. Bellshaw, N. Zotev, M. Liang, S. Carbajo, J. Koglin, J. S. Robinson, S. Boutet, A. Kirrander, M. P. Minitti, and P. M. Weber, A deep UV trigger for ground-state ring-opening dynamics of 1,3-cyclohexadiene, Sci. Adv. **5**, eaax6625 (2019).

[6] A. R. Attar, A. Bhattacherjee, C. D. Pemmaraju, K. Schnorr, K. D. Closser, D. Prendergast, and S. R. Leone, Femtosecond x-ray spectroscopy of an electrocyclic ring-opening reaction, Science **356**, 54 (2017).

[7] T. J. A. Wolf *et al.*, The photochemical ring-opening of 1,3-cyclohexadiene imaged by ultrafast electron diffraction, Nat. Chem. **11**, 504 (2019).

[8] F. Rudakov and P. M. Weber, Ground state recovery and molecular structure upon ultrafast transition through conical intersections in cyclic dienes, Chem. Phys. Lett. **470**, 187 (2009).

[9] S. Adachi, M. Sato, and T. Suzuki, Direct observation of ground-state product formation in a 1,3-cyclohexadiene ring-opening reaction, J. Phys. Chem. Lett. **6**, 343 (2015).

[10] M. Tudorovskaya, R. Minns, and A. Kirrander, Effect of probe energy and competing pathways on time-resolved photoelectron spectroscopy signals: The ring-opening of 1,3-cyclohexadiene, Phys. Chem. Chem. Phys. **20**, 17714 (2018).

[11] S. Pathak *et al.*, Tracking the ultraviolet-induced photochemistry of thiophenone during and after ultrafast ring opening, Nat. Chem. **12**, 795 (2020).

[12] B. C. Arruda and R. J. Sension, Ultrafast polyene dynamics: The ring opening of 1,3-cyclohexadiene derivatives, Phys. Chem. Chem. Phys. **16**, 4439 (2014).

[13] E. Havinga and J. Schlatmann, Remarks on the specificities of the photochemical and thermal transformations in the vitamin D field, Tetrahedron **16**, 146 (1961).

[14] P. M. Woods, T. J. Millar, E. Herbst, and A. A. Zijlstra, The chemistry of protoplanetary nebulae, Astron. Astrophys. **402**, 189 (2003).

[15] H. M. Boechat-Roberty, R. Neves, S. Pilling, A. F. Lago, and G. G. B. De Souza, Dissociation of the benzene molecule by ultraviolet and soft X-rays in circumstellar environment, Mon. Not. R. Astron. Soc. **394**, 810 (2009).

[16] M. Alagia, P. Candori, S. Falcinelli, M. S. P. Mundim, F. Pirani, R. Richter, M. Rosi, S. Stranges, and F. Vecchiocattivi, Dissociative double photoionization of singly deuterated benzene molecules in the 26 33 eV energy range, J. Chem. Phys. **135**, 144304 (2011).

[17] M. Alagia, P. Candori, S. Falcinelli, F. Pirani, M. S. P. Mundim, R. Richter, M. Rosi, S. Stranges, and F. Vecchiocattivi, Dissociative double photoionization of benzene molecules in the 2633 eV energy range, Phys. Chem. Chem. Phys. **13**, 8245 (2011).

[18] M. C. E. Galbraith, C. T. L. Smeenk, G. Reitsma, A. Marciniak, V. Despré, J. Mikosch, N. Zhavoronkov, M. J. J. Vrakking, O. Kornilov, and F. Lépine, XUV-induced reactions in benzene on sub-10 fs timescale: Nonadiabatic relaxation and proton migration, Phys. Chem. Chem. Phys. **19**, 19822 (2017).

[19] F. A. Rajgara, M. Krishnamurthy, D. Mathur, T. Nishide, H. Shiromaru, and N. Kobayashi, Coulombic and non-Coulombic fragmentation of highly charged benzene, J. Phys. B **37**, 1699 (2004).

[20] V. R. Bhardwaj, K. Vijayalakshmi, and D. Mathur, Dissociative ionization of benzene in intense laser fields of picosecond duration, Phys. Rev. A **59**, 1392 (1999).

[21] A. H. Winney, Y. F. Lin, S. K. Lee, P. Adhikari, and W. Li, State-resolved three-dimensional electron-momentum correlation in nonsequential double ionization of benzene, Phys. Rev. A **93**, 031402(R) (2016).

[22] P. J. Richardson, J. H. D. Eland, and P. Lablanquie, Charge separation reactions of doubly charged benzene ions, Org. Mass Spectrom. **21**, 289 (1986).

[23] N. Neumann, D. Hant, L. P. H. Schmidt, J. Titze, T. Jahnke, A. Czasch, M. S. Schöffler, K. Kreidi, O. Jagutzki, H. Schmidt-Böcking, and R. Dörner, Fragmentation Dynamics of CO_2^{3+} Investigated by Multiple Electron Capture in Collisions with Slow Highly Charged Ions, Phys. Rev. Lett. **104**, 103201 (2010).

[24] C. Wu, C. Wu, D. Song, H. Su, Y. Yang, Z. Wu, X. Liu, H. Liu, M. Li, Y. Deng, Y. Liu, L.-Y. Peng, H. Jiang, and Q. Gong, Nonsequential and Sequential Fragmentation of CO_2^{3+} in Intense Laser Fields, Phys. Rev. Lett. **110**, 103601 (2013).

[25] E. Wang, X. Shan, Z. Shen, M. Gong, Y. Tang, Y. Pan, K.-C. Lau, and X. Chen, Pathways for nonsequential and sequential fragmentation of CO_2^{3+} investigated by electron collision, Phys. Rev. A **91**, 052711 (2015).

[26] J. Rajput, T. Severt, B. Berry, B. Jochim, P. Feizollah, B. Kaderiya, M. Zohrabi, U. Ablikim, F. Ziaee, K. Raju P., D. Rolles, A. Rudenko, K. D. Carnes, B. D. Esry, and I. Ben-Itzhak, Native Frames: Disentangling Sequential from Concerted Three-Body Fragmentation, Phys. Rev. Lett. **120**, 103001 (2018).

[27] U. Ablikim, C. Bomme, E. Savelyev, H. Xiong, R. Kushawaha, R. Boll, K. Amini, T. Osipov, D. Kilcoyne, A. Rudenko, N. Berrah, and D. Rolles, Isomer-dependent fragmentation dynamics of inner-shell photoionized difluoroiodobenzene, Phys. Chem. Chem. Phys. **19**, 13419 (2017).

[28] A. Matsuda, M. Fushitani, R. D. Thomas, V. Zhaunerchyk, and A. Hishikawa, Multiple explosion pathways of the deuterated

[29] benzene trication in 9-fs intense laser fields, J. Phys. Chem. A **113**, 2254 (2009).

[29] A. Hishikawa, A. Iwamae, and K. Yamanouchi, Ultrafast Deformation of the Geometrical Structure of CO_2 Induced in Intense Laser Fields, Phys. Rev. Lett. **83**, 1127 (1999).

[30] K. Bartschat and M. J. Kushner, Electron collisions with atoms, ions, molecules, and surfaces: Fundamental science empowering advances in technology, Proc. Natl. Acad. Sci. USA **113**, 7026 (2016).

[31] E. Alizadeh, T. M. Orlando, and L. Sanche, Biomolecular damage induced by ionizing radiation: The direct and indirect effects of low-energy electrons on DNA, Annu. Rev. Phys. Chem. **66**, 379 (2015).

[32] S. M. Pimblott and J. A. LaVerne, Production of low-energy electrons by ionizing radiation, Radiat. Phys. Chem. **76**, 1244 (2007).

[33] L. Campbell and M. Brunger, Electron collisions in atmospheres, Int. Rev. Phys. Chem. **35**, 297 (2016).

[34] R. Dalitz, CXII. On the analysis of τ-meson data and the nature of the τ-meson, London, Edinburgh Dublin Philos. Mag. J. Sci. **44**, 1068 (1953).

[35] J. Eland, The dynamics of three-body dissociations of dications studied by the triple coincidence technique PEPIPICO, Mol. Phys. **61**, 725 (1987).

[36] J. Ullrich, R. Moshammer, A. Dorn, R. Dörner, L. P. H. Schmidt, and H. Schmidt-Böcking, Recoil-ion and electron momentum spectroscopy: Reaction-microscopes, Rep. Prog. Phys. **66**, 1463 (2003).

[37] X. Ren, T. Pflüger, M. Weyland, W. Y. Baek, H. Rabus, J. Ullrich, and A. Dorn, An (e, 2e + ion) study of low-energy electron-impact ionization and fragmentation of tetrahydrofuran with high mass and energy resolutions, J. Chem. Phys. **141**, 134314 (2014).

[38] H. B. Schlegel, J. M. Millam, S. S. Iyengar, G. A. Voth, A. D. Daniels, G. E. Scuseria, and M. J. Frisch, *Ab initio* molecular dynamics: Propagating the density matrix with Gaussian orbitals, J. Chem. Phys. **114**, 9758 (2001).

[39] S. S. Iyengar, H. B. Schlegel, J. M. Millam, G. A. Voth, G. E. Scuseria, and M. J. Frisch, *Ab initio* molecular dynamics: Propagating the density matrix with Gaussian orbitals. II. Generalizations based on mass-weighting, idempotency, energy conservation and choice of initial conditions, J. Chem. Phys. **115**, 10291 (2001).

[40] H. B. Schlegel, S. S. Iyengar, X. Li, J. M. Millam, G. A. Voth, G. E. Scuseria, and M. J. Frisch, *Ab initio* molecular dynamics: Propagating the density matrix with Gaussian orbitals. III. Comparison with Born-Oppenheimer dynamics, J. Chem. Phys. **117**, 8694 (2002).

[41] R. M. Richard, M. S. Marshall, O. Dolgounitcheva, J. V. Ortiz, J.-L. Brédas, N. Marom, and C. D. Sherrill, Accurate ionization potentials and electron affinities of acceptor molecules I. Reference data at the CCSD(T) complete basis set limit, J. Chem. Theory Comput. **12**, 595 (2016).

[42] T. S. Zyubin, G.-S. Kim, A. M. Mebel, S. H. Lin, and A. D. Bandrauk, Ab initio/RRKM study of dissociation mechanism of benzene trication, J. Theor. Comput. Chem. **2**, 205 (2003).

[43] O. Vendrell, S. D. Stoychev, and L. S. Cederbaum, Generation of highly damaging H_2O^+ radicals by inner valence shell ionization of water, ChemPhysChem **11**, 1006 (2010).

[44] M. J. Frisch *et al.*, GAUSSIAN 16, revision A.03 (Gaussian Inc., Wallingford CT, 2016).

[45] F. Tarantelli, A. Sgamellotti, L. S. Cederbaum, and J. Schirmer, Theoretical investigation of many dicationic states and the Auger spectrum of benzene, J. Chem. Phys. **86**, 2201 (1987).

[46] J. H. D. Eland, M. Hochlaf, P. Linusson, E. Andersson, L. Hedin, and R. Feifel, Triple ionization spectra by coincidence measurements of double Auger decay: The case of ocs, J. Chem. Phys. **132**, 014311 (2010).

[47] D. E. Ramaker, The past, present, and future of Auger line shape analysis, Crit. Rev. Solid State Mater. Sci. **17**, 211 (1991).

[48] S. Hsieh and J. H. D. Eland, Reaction dynamics of three-body dissociations in triatomic molecules from single-photon double ionization studied by a time- and position-sensitive coincidence method, J. Phys. B **30**, 4515 (1997).

[49] A. Hishikawa, H. Hasegawa, and K. Yamanouchi, Sequential three-body Coulomb explosion of Cs_2 in intense laser fields appearing in momentum correlation map, Chem. Phys. Lett. **361**, 245 (2002).